Ginzburg-Landau theory of solvation in polar fluids: Ion distribution around an interface

Akira Onuki

Department of Physics, Kyoto University, Kyoto 606-8502, Japan

We present a Ginzburg-Landau theory of solvation of ions in polar binary mixtures. The solvation free energy arising from the ion-dipole interaction can strongly depend on the composition and the ion species. Most crucial in phase separation is then the difference in the solvation free energy between the two phases, which is the origin of the Galvani potential difference known in electrochemistry. We also take into account an image potential acting on each ion, which arises from inhomogeneity in the dielectric constant and is important close to an interface at very small ion densities. Including these solvation and image interactions, we calculate the ion distributions and the electric potential around an interface with finite thickness. In particular, on approaching the critical point, the ion density difference between the two phases becomes milder. The critical temperature itself is much shifted even by a small amount of ions. We examine the surface tension in the presence of ions in various cases.

I. INTRODUCTION

Charge effects have long been discussed extensively in electrolytes, polyelectrolytes, gels, DNA, and so on [1,2]. In most of the physics literature, charged particles interact via the Coulombic potential in a fluid with a homogeneous dielectric constant ε. In the chemistry literature, on the other hand, attention has been paid to the microscopic molecular interactions between an ion and the surrounding solvent molecules [3,4], which give rise to a chemical potential contribution of ions dependent on the solvent density (composition for mixtures) and the temperature T. For a microscopic ion, such as Na$^+$ or Cl$^-$ in a polar fluid, it is the so-called solvation free energy (hydration free energy in water or aqueous solutions) per ion arising from the ion-dipole interaction under the influence of hydrogen bonding [5,6]. In this paper, it will be called the solvation chemical potential and will be written as μ_{sol}^i dependent on the ion species i. It is a crucial quantity in understanding the degree of solubility of ions in polar solvents [3,4]. Since μ_{sol}^i strongly depends on the solvent density or composition and can much exceed k_BT, it should play various important roles particularly in the formation of inhomogeneous structures, which has been one of the main subjects in soft matter physics.

As a classic example, the Born theory [7] takes into account polarization around an ion using the linear dielectric constant ε and gives the solvation free energy in the form,

$$(\mu_{\text{sol}}^i)_{\text{Born}} = Z^2 e^2/2\varepsilon R_{\text{ion}}^i, \qquad (1.1)$$

where Ze is the ion charge and R_{ion}^i is the microscopic ion radius (of order 1 Å for Na$^+$) [3,8]. For water, ε is of order 1 in gas and of order 100 in liquid at room temperatures, so its density dependence is very strong [9]. For mixtures of two fluid components, A and B, ε changes from the dielectric constant ε_B of the less polar component to that ε_A of the more polar component with increasing the volume fraction ϕ of the more polar component [4,10]. However, it is well known that the Born formula neglects electrostriction [3,11] and nonlinear dielectric saturation [12–14] in the vicinity of

an ion and is in many cases an overestimation. For mixtures, the former effect means that molecules of the more polar component accumulate around an ion to form the solvation shell [3,4]. The latter effect means that the effective dielectric constant in the vicinity of an ion should be smaller than in the bulk. Nevertheless, the Born formula demonstrates strong dependence of μ_{sol}^i on the solvent density or composition.

Let a fluid be phase separated into a highly polar phase α and a less polar phase β. Generally, μ_{sol}^i takes different values in the two bulk phases and these values depend on the ion species i (Na$^+$ or Cl$^-$, for example), so they are written as $\mu_{\text{sol}}^{i\alpha}$ and $\mu_{\text{sol}}^{i\beta}$. In the electrochemistry literature [15–19], the chemical-potential difference

$$\Delta\mu_{\alpha\beta}^i = \mu_{\text{sol}}^{i\beta} - \mu_{\text{sol}}^{i\alpha} \qquad (1.2)$$

between the two phases is called the standard Gibbs transfer energy (usually per mole, but per ion in this paper). Using data of $\Delta\mu_{\alpha\beta}^i$ on water+nitrobenzene [17] (with α being a water-rich phase), we estimate $\Delta\mu_{\alpha\beta}^i/k_BT$ as 13.6 for Na$^+$, 10.6 for K$^+$, 11.3 for Br$^-$, and 7.46 for I$^-$, where we set T =300 K. Notice that if $\Delta\mu_{\alpha\beta}^i \gg k_BT$, there arises a large difference in the ion density between the two phases. Furthermore, since $\Delta\mu_{\alpha\beta}^i$ depends on the ion species, there can be an electric double layer at the interface, which then leads to an electric potential difference across the interface, called the Galvani potential difference. We also note that $\Delta\mu_{\alpha\beta}^i$ is a parameter dramatically influencing the nucleation process when a small amount of ions are doped in a metastable polar fluid [20,21]. Recently, $\Delta\mu_{\alpha\beta}^i$ was calculated between gaseous water (phase β) and liquid water (phase α), which is much larger than k_BT far below the critical point [22].

It has also long been known that the surface tension of a water-air interface increases with increasing the salt density [23–30]. The ion density nearly vanishes in the air region, obviously due to very large $\Delta\mu_{\alpha\beta}^i/k_BT$. Here, phase α is salty water and phase β is air. It has been argued that ions in water should be repelled away from the interface by the image

charges in air [24,25]. This leads to a depletion of the ion density near the interface and an increase of the surface tension,

$$\Delta\gamma = k_B T n_{\text{salt}} \lambda_s, \tag{1.3}$$

where n_{salt} is the salt density in the bulk water and λ_s is the effective thickness of the ion-free layer. This is in marked contrast to the role of surfactant molecules, which serve to decrease the surface tension [31]. For example, λ_s is about 6 Å for NaCl at room temperatures [29]. The image interaction comes into play in λ_s at low salt densities, where $\Delta\gamma$ itself is small, however. Here, we mention microscopic calculations of the ion distributions at a water-air interface [6] (see discussions in Sec. III).

We stress that the strong density or composition dependence of μ_{sol}^i gives rise to a number of unexplored physical effects, particularly in two-phase states. As a paper in this direction, we will examine the ion distributions around an interface in the scheme of Ginzburg-Landau theory [22,32,33]. In Sec. II, we will present our scheme accounting for electrostatics with inhomogeneous ε, solvation effects, and image forces. In Sec. III, we will explain our numerical scheme and show profiles of the electric field in a parallel-plate capacitor. In Sec. IV, we will present a number of general relations and show numerical results of the interface structure. In Appendix A, we will summarize the calculations of the structure factor of the composition fluctuations and the effective interaction potentials among the ions in near-critical one-phase states.

II. GINZBURG-LANDAU THEORY

Let us consider a polar binary mixture with a small amount of salt composed of two species of ions. The volume fraction of the more polar component A will be written as $\phi(\mathbf{r})$. The ion densities are $n_1(\mathbf{r})$ and $n_2(\mathbf{r})$. In the continuum limit, ϕ, n_1, and n_2 are smooth variables coarse-grained on the microscopic level, and we will set up the Ginzburg-Landau free energy F as a functional of these variables. We will assume that the ion densities are small and will neglect formation of dipole pairs [2,34]. We divide F into three parts as

$$F = F_e + F_{\text{ch}} + F_{\text{im}} \tag{2.1}$$

and will explain each term in the following.

A. Electrostatics

We assume that the dielectric constants ε_A and ε_B of the two components are significantly different and concentration dependence of the dielectric constant of the mixture may be expressed as [10]

$$\varepsilon(\phi) = \varepsilon_0 + \varepsilon_1 \phi, \tag{2.2}$$

where ε_0 and ε_1 are positive constants with [35]

$$\varepsilon_0 = \varepsilon_B, \quad \varepsilon_1 = \varepsilon_A - \varepsilon_B > 0. \tag{2.3}$$

Empirically, ε can be expressed roughly as a linear function of the concentration in many mixtures investigated so far
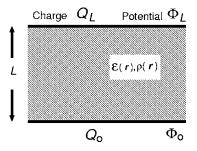

FIG. 1. Ionic fluid between parallel metal plates with space-dependent dielectric constant ε and charge density ρ. Surface charges Q_L and Q_0 are fixed.

[4,10]. Hereafter, $\mathbf{E} = -\nabla\Phi$ is the electric field and $\mathbf{D} = \varepsilon\mathbf{E}$ is the electric induction, where Φ is the electric potential. They satisfy

$$\nabla \cdot \mathbf{D} = -\nabla \cdot \varepsilon(\phi)\nabla\Phi = 4\pi\rho. \tag{2.4}$$

The charge density $\rho(\mathbf{r})$ is written as

$$\rho = e(Z_1 n_1 - Z_2 n_2), \tag{2.5}$$

where e is the elementary charge and the two ion species have charges, $Q_1 = Z_1 e$ and $Q_2 = -Z_2 e$.

As a typical experimental geometry, our fluid system is inserted between two parallel metal plates with area S and separation distance L as shown in Fig. 1. We assume $S^{1/2} \gg L$ and neglect the effects of edge fields, for simplicity. The z axis is taken perpendicularly to the plates. The surface charge densities at the upper plate at $z = L$ and the lower plate at $z = 0$ are σ_L and σ_0, respectively. The total charges on the plates are $Q_L = S\sigma_L$ and $Q_0 = S\sigma_0$, respectively. The charge neutrality condition is written as

$$Q_L + Q_0 + \int d\mathbf{r}\rho = 0, \tag{2.6}$$

where the space integral $\int d\mathbf{r}(\cdots)$ is within the fluid region $(0 < z < L)$. In this paper, we fix σ_L and σ_0 and consider the electrostatic free energy dependent on inhomogeneous ε and ρ [33,36],

$$F_e = \int d\mathbf{r}\frac{\varepsilon(\phi)}{8\pi}E^2 = \int d\mathbf{r}\frac{1}{8\pi}\mathbf{E} \cdot \mathbf{D}. \tag{2.7}$$

On the plates at $z = 0$ and L, Φ takes laterally homogeneous values Φ_0 and Φ_L, and

$$D_z(0) = 4\pi\sigma_0, \quad D_z(L) = -4\pi\sigma_L. \tag{2.8}$$

The potential difference $\Phi_L - \Phi_0$ is a functional of $\varepsilon(\mathbf{r})$ and $\rho(\mathbf{r})$. We next change $\varepsilon(\mathbf{r})$ and $\rho(\mathbf{r})$ infinitesimally by $\delta\varepsilon(\mathbf{r})$ and $\delta\rho(\mathbf{r})$ and use the relation,

$$\delta(\varepsilon E^2) = -E^2\delta\varepsilon + 2\mathbf{E} \cdot \delta\mathbf{D} = -E^2\delta\varepsilon - 2\nabla \cdot (\Phi\delta\mathbf{D})$$
$$+ 8\pi\Phi\delta\rho. \tag{2.9}$$

Because δD_z should vanish on the boundaries at fixed surface charges, we find

$$\delta F_e = \int d\mathbf{r} \left[-\frac{1}{8\pi} \mathbf{E}^2 \delta \varepsilon + \Phi \delta \rho \right]. \qquad (2.10)$$

Under Eqs. (2.2) and (2.5), the above relation yields

$$\frac{\delta F_e}{\delta \phi} = -\frac{\varepsilon_1}{8\pi} \mathbf{E}^2, \qquad (2.11)$$

$$\frac{\delta F_e}{\delta n_1} = Z_1 e \Phi, \qquad \frac{\delta F_e}{\delta n_2} = -Z_2 e \Phi. \qquad (2.12)$$

B. Solvation interaction

In Eq. (2.1), the second term F_{ch} is the chemical part,

$$F_{\mathrm{ch}} = \int d\mathbf{r} \left\{ f(\phi) + \frac{1}{2} C |\nabla \phi|^2 + \sum_{i=1,2} [k_B T n_i (\ln(v_0 n_i) - 1) \right.$$
$$\left. + n_i \mu_{\mathrm{sol}}^i(\phi)] \right\}. \qquad (2.13)$$

The free energy density $f = f(\phi)$ is given by the Hildebrand (or Bragg-Williams) expression [31,37],

$$\frac{v_0 f}{k_B T} = \phi \ln \phi + (1 - \phi) \ln(1 - \phi) + \chi \phi (1 - \phi), \quad (2.14)$$

where v_0 is the molecular volume and χ is the interaction parameter dependent on the temperature T. The molecules of the two components have a common size

$$a = v_0^{1/3} \qquad (2.15)$$

on the order of a few angstroms. Here the volume fraction of the ions is neglected [38]. The critical-point values of ϕ and χ in the absence of ions are

$$\phi_c = 1/2, \quad \chi_c = 2, \qquad (2.16)$$

respectively, in the mean-field theory. That is, as $\chi \to 2$, $2 - \chi = A(T - T_c^0)$ with A being a constant and T_c^0 being the critical temperature without ions. It is convenient to define the order parameter by

$$\psi = \phi - 1/2, \qquad (2.17)$$

which vanishes at the critical point without ions. The coefficient C of the gradient term is of order $k_B T/a$ and we will use a simple form [31],

$$C = k_B T \chi / a. \qquad (2.18)$$

Near the critical point, we may well use the expansion form $f = \tau \psi^2/2 + u \psi^4/4$ [see Eq. (4.49) below].

In the second line of Eq. (2.13), $\mu_{\mathrm{sol}}^i(\phi)$ ($i = 1, 2$) are the chemical potential contributions of ions due to interactions between the ions and the solvent molecules and depend on ϕ and T. In this paper, we simply assume the linear dependence,

$$\mu_{\mathrm{sol}}^i(\phi) = \mu_c^i - k_B T g_i \psi \quad (i = 1, 2). \qquad (2.19)$$

The first terms are irrelevant constants in F when the ion numbers are conserved quantities. It follows the relation

$\Delta \mu_{\alpha\beta}^i = k_B T g_i \Delta \phi$ with $\Delta \phi$ being the composition difference between the two phases. The linear dependence here and that in $\varepsilon(\phi)$ in Eq. (2.2) are adopted to gain the physical consequences in the simplest manner and should not be taken too seriously. We then have the bilinear solvation interaction ($\propto \psi n_i$) in F among the ions and the composition fluctuations [32,39]. In aqueous solutions, the coupling constants g_i are positive for hydrophilic ions and can much exceed unity for small ions such as Li^+ or Na^+, while they should be negative for hydrophobic organic ions [14]. They should be larger for small multivalent ions such as Mg^{2+} or Al^{3+}. As will be summarized in Appendix A, we recently examined the effect of this solvation interaction in near-critical one-phase states [32]. In this work, its effect will be examined in two-phase states. In addition, $1/\varepsilon(\phi)$ in the Born formula Eq. (1.1) may be expanded in powers of ψ near the critical point to give [33,40]

$$(g_i)_{\mathrm{Born}} = Z_i^2 e^2 \varepsilon_1 / 2 k_B T \varepsilon_c^2 R_{\mathrm{ion}}^i, \qquad (2.20)$$

where ε_c is the dielectric constant at the critical composition and R_{ion}^i is the ion radius of the species i. However, because of the defects of the Born theory, we will treat g_i as free parameters not using Eq. (2.20).

Hydrophilic ions and several water molecules (those of the more polar component in a mixture) form a complex structure and its effective radius R_{shell}^i, called the solvation (hydration) shell radius, can be a few angstroms and is larger than the bare ion radius R_{ion}^i [3,4]. In a number of experiments, water molecules have been extracted together with hydrophilic ions in a less polar phase with a small water concentration. In nitrobenzene (NB) -water at room temperatures, the number of coextracted water molecules in a NB-rich phase was estimated to be 4 for Na^+, 6 for Li^+, and 15 for Ca^{2+} [14]. For liquid-vapor systems, where ions are absent in vapor, Levin and Flores-Mena [27] argued that ions in liquid cannot approach the interface within the distance of R_{shell}^i in the thin interface limit $\xi \to 0$. In our theory, R_{shell}^i does not appear explicitly, but ions in the more polar region are strongly repelled from the interface outside the distance of ξ for large g_i. Therefore, our present treatment is justified in the case $\xi \gtrsim R_{\mathrm{shell}}^i$.

C. Image interaction

As will be discussed in Appendix B, the last term F_{im} arises from a deformation of the self-interaction of ions due to inhomogeneous ε. It originates from the discrete nature of ions, while the electric field Φ in Eq. (2.4) is produced by the smoothly coarse-grained charge density ρ. If an ion is close to an interface, the chemical potential contribution $\mu_{\mathrm{im}}^i = \delta F_{\mathrm{im}}/\delta n_i$ is the so-called image potential in the previous papers [24–26]. This interaction can be important close to an interface far below the critical point or a boundary wall.

In this paper, assuming weak or moderate spatial variations of ε, we derive the following integral form,

$$F_{\mathrm{im}} = \int \int d\mathbf{r} d\mathbf{r}' m(\mathbf{r}) \nabla' I(\mathbf{r}, \mathbf{r}') \cdot \nabla' \phi(\mathbf{r}'), \qquad (2.21)$$

where $\nabla' = \partial/\partial \mathbf{r}'$. We define a new variable,

$$m = Z_1^2 n_1 + Z_2^2 n_2, \qquad (2.22)$$

which coincides with the total ion density,

$$n = n_1 + n_2, \qquad (2.23)$$

in the monovalent case $Z_1 = Z_2 = 1$. If the boundary effects are neglected, the function $I(\mathbf{r}, \mathbf{r}')$ depends only on the difference $\mathbf{r} - \mathbf{r}'$ as

$$I(\mathbf{r}, \mathbf{r}') = \frac{B_0}{|\mathbf{r} - \mathbf{r}'|^2} e^{-2\kappa|\mathbf{r} - \mathbf{r}'|}. \qquad (2.24)$$

Near the critical point, the coefficient B_0 is given by

$$B_0 = e^2 \varepsilon_1 / 8\pi \varepsilon_c^2, \qquad (2.25)$$

where $\varepsilon_c = \varepsilon_0 + \varepsilon_1/2$ is the dielectric constant at the critical point and κ is the Debye-Hückel wave number. When the ion densities vary significantly in space in a phase-separated state, κ may be taken as the space-dependent local value [see sentences below Eq. (3.8)] [24] or the value in the more polar phase [25].

In our numerical analysis, we will set $\varepsilon_1 = 4\varepsilon_0/3$ or $\varepsilon_1 = 4\varepsilon_c/5$ for $\phi_c = 1/2$. Then $|\varepsilon_1 \psi|/\varepsilon_c$ is at most 0.4 in strong segregation of composition. Our one-dimensional form of F_{im} to be presented in Eq. (3.7) below overestimates the usual expression in the case $\varepsilon_1 \gg \varepsilon_0$ [25] by a factor of 2 in strong segregation. See Appendix B.

D. Chemical potentials and equilibrium

We calculate the chemical potentials $\mu_1 = \delta F/\delta n_1$ and $\mu_2 = \delta F/\delta n_2$ of the ions and $h = \delta F/\delta \phi$. Here $h = (\mu_A - \mu_B)/v_0$ in terms of the chemical potentials μ_A and μ_B of the two components of the mixture [37]. Using Eqs. (2.11) and (2.12), we obtain

$$\mu_1 = k_B T \ln(v_0 n_1) + Z_1 e\Phi + \mu_{\text{sol}}^1 + \mu_{\text{im}}^1,$$

$$\mu_2 = k_B T \ln(v_0 n_2) - Z_2 e\Phi + \mu_{\text{sol}}^2 + \mu_{\text{im}}^2. \qquad (2.26)$$

From Eqs. (2.11), (2.13), and (2.19), we find

$$h = f'(\phi) - C\nabla^2\phi - \frac{\varepsilon_1}{8\pi}\mathbf{E}^2 - k_B T \sum_{i=1,2} g_i n_i + h_{\text{im}}, \qquad (2.27)$$

where $f' = \partial f/\partial \phi$. In these expressions, the last two terms arise from the solvation and image interactions, respectively, and we define

$$\mu_{\text{im}}^i = \frac{\delta F_{\text{im}}}{\delta n_i}, \quad h_{\text{im}} = \frac{\delta F_{\text{im}}}{\delta \phi}. \qquad (2.28)$$

If Eq. (2.24) is used with a constant κ, we have

$$\mu_{\text{im}}(\mathbf{r}) \equiv \mu_{\text{im}}^i/Z_i^2 = \int d\mathbf{r}' \nabla' I(\mathbf{r}, \mathbf{r}') \cdot \nabla' \psi(\mathbf{r}'),$$

$$h_{\text{im}}(\mathbf{r}) = \int d\mathbf{r}' \nabla' I(\mathbf{r}, \mathbf{r}') \cdot \nabla' m(\mathbf{r}'). \qquad (2.29)$$

In our numerical analysis, we have used these expressions in Eqs. (2.26) and (2.27) for simplicity [see Eq. (3.7)].

In equilibrium, μ_1, μ_2, and h are constants in space. The ion distributions are written in terms of the potential Φ and the order parameter $\psi = \phi - 1/2$ as

$$n_1 = n_1^0 \exp\left[g_1 \psi - \frac{Z_1}{k_B T}(e\Phi + Z_1 \mu_{\text{im}}) \right],$$

$$n_2 = n_2^0 \exp\left[g_2 \psi + \frac{Z_2}{k_B T}(e\Phi - Z_2 \mu_{\text{im}}) \right], \qquad (2.30)$$

where we have used Eq. (2.19) for μ_{sol}^i and Eq. (2.29) for μ_{im}^i. The coefficients n_1^0 and n_2^0 are determined from the conditions $N_1 = \int d\mathbf{r} n_1 = \text{const.}$ and $N_2 = \int d\mathbf{r} n_2 = \text{const.}$

III. NUMERICAL METHOD AND ONE-DIMENSIONAL PROFILES WITH BOUNDARIES

We consider one-dimensional equilibrium situations in which all the quantities in F depend only on z. We introduce normalized ion densities by

$$c_1(z) = v_0 n_1(z), \quad c_2(z) = v_0 n_2(z). \qquad (3.1)$$

As typical values, if $n_1 = 10^{-4}$ mole/cm^3 and $a = 3.1$ Å, we obtain $c_1 = 1.8 \times 10^{-3}$. We simply call c_1 and c_2 as concentrations, supposing $R_{\text{shell}}^i \sim a$. We also introduce a dimensionless electric potential,

$$U(z) = e\Phi(z)/k_B T. \qquad (3.2)$$

In Appendix C, we will write down the equilibrium equations for $\psi = \phi - 1/2$, c_1, c_2, and U. There appears a parameter A representing the strength of the charges,

$$A = \pi e^2/4a\varepsilon_c k_B T = \pi \ell_{Bc}/4a, \qquad (3.3)$$

where $a = v_0^{1/3}$ is the molecular size and

$$\ell_{Bc} = e^2/\varepsilon_c k_B T \qquad (3.4)$$

is the Bjerrum length at the critical dielectric constant.

Our numerical calculations are all in the monovalent case $Z_1 = Z_2 = 1$. We integrated the time-dependent equations,

$$\frac{\partial \phi}{\partial t} = -\frac{\delta F}{\delta \phi} + \left\langle \frac{\delta F}{\delta \phi} \right\rangle, \qquad (3.5)$$

$$\frac{\partial U}{\partial t} = \nabla \cdot \varepsilon \nabla U + 4\pi\rho, \qquad (3.6)$$

until steady solutions were nearly reached, where $\langle \cdots \rangle$ is the space average. Notice that h in Eq. (2.27) becomes equal to the space average $\langle \delta F/\delta \phi \rangle$ in equilibrium. Thus the steady solutions of Eqs. (3.5) and (3.6) are the equilibrium solutions. We used h_{im} in Eq. (2.29) as $\delta F_{\text{im}}/\delta \phi$ in $\delta F/\delta \phi$ and n_1 and n_2 in Eq. (2.30) to calculate $m = n$ and ρ. These equations do not represent the real dynamics, but conveniently give the equilibrium solutions.

In $\mu_{\text{im}}(z)$ and $h_{\text{im}}(z)$ in Eq. (2.29) we replace $\exp(-2\kappa|\mathbf{r} - \mathbf{r}'|)$ in $I(\mathbf{r}, \mathbf{r}')$ by $\exp(-2\kappa|z - z'|)$ for simplicity and integrate over x' and y' to obtain
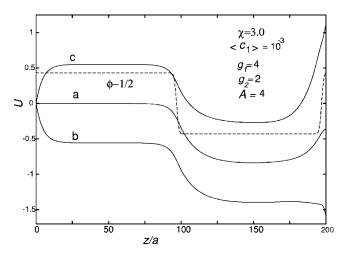
FIG. 2. Normalized electric potential $U(z) = e\Phi(z)/k_BT$ between parallel plates with $L = 200a$, where we set $\Phi(0) = 0$. The surface charge $\sigma_0 (= -\sigma_L)$ is 0 (a), $2.5 \times 10^{-3} e/a^2$ (b), and $-2.5 \times 10^{-3} e/a^2$ (c). The curve of $\psi(z) = \phi(z) - 1/2$ (broken line) indicates the presence of an interface in the middle and a wetting layer in contact with the wall at $z = L$.

$$\mu_{\text{im}}(z) = 2\pi B_0 \int \frac{dz'}{z - z'} e^{-2\kappa|z - z'|} \left| \frac{d}{dz'} \psi(z'), \right. \quad (3.7)$$

where B_0 is given in Eq. (2.25). See Eq. (B9). The $h_{\text{im}}(z)$ is obtained if $\psi(z')$ is replaced by $m(z')$ in Eq. (3.7). We neglected the image interaction in the regions $z < 20a$ and $L - z < 20a$ close to the boundaries. As the Debye-Hückel wave number in Eq. (3.7), we used its local value in the monovalent case,

$$\kappa(z) = [4\pi n(z) e^2 / \varepsilon(\phi(z)) k_BT]^{1/2}. \quad (3.8)$$

We also performed numerical analysis by setting κ equal to the bulk value κ_α in Eq. (4.2). A noticeable difference can be seen only in the long-distance behavior of the electric potential Φ in the phase β at very small ion densities (see Fig. 13 below). The calculated values of the excess surface tension are different between these two choices only by a few percents.

In Fig. 2, we show numerically calculated profiles of the normalized electric potential $U(z)$, for $\chi = 3$, $g_1 = 4$, $g_2 = 2$, and $A = 4$ in the geometry of Fig. 1 with $L = 200a$. The space averages are $\langle \psi \rangle = 0$ and $\langle c_1 \rangle = \langle c_2 \rangle = 0.001$. The three curves correspond to the surface charge densities given by $\sigma_0 = -\sigma_L = 0$ (a), $2.5 \times 10^{-3} e/a^2$ (b), and $-2.5 \times 10^{-3} e/a^2$ (c). Note that $D_z = -\varepsilon d\Phi/dz$ satisfies the boundary condition in Eq. (2.8). On the composition deviation $\psi = \phi - 1/2$, we impose the boundary condition [41],

$$\psi = \pm (2\sqrt{2})^{-1} a\psi' + 0.5, \quad (3.9)$$

where $\psi' = d\psi/dz$, + is for $z = 0$, and − is for $z = L$. Under Eq. (3.9), the boundary walls are wetted by the more polar phase. The electric potential exhibits a jump near the interface, whose spatial scale is of the order of the screening length $1/\kappa$ longer than the interface thickness ξ in the present case. This suggests the presence of an electric double layer at the

interface, as will be discussed in Sec. IV B. The surface charges σ_0 and σ_L are screened by a fraction of the ions in the fluid.

IV. PLANAR INTERFACE

From Fig. 2, we can see that the interface is not affected by the surface charges and the wetting layer as long as the distances to the boundaries are much longer than the screening length. We focus our attention to a planar interface separating two phases α and β. The volume fraction ϕ_α in the phase α is larger than that ϕ_β in the phase β, so the dielectric constant is larger in the phase α than in the phase β,

$$\varepsilon_\alpha = \varepsilon_c + \varepsilon_1 \psi_\alpha > \varepsilon_\beta = \varepsilon_c + \varepsilon_1 \psi_\beta. \quad (4.1)$$

The interface structure is determined by the six dimensionless parameters, χ, g_1, g_2, ϵ_1/ϵ_c, A, and the bulk ion concentration $c_{1\alpha}$ in the phase α. In this paper, we set $\epsilon_1/\epsilon_c = 0.8$, but the other parameters are varied.

A. General relations

We assume that there are significant ion densities in the two phases such that the bulk screening lengths $1/\kappa_\alpha$ and $1/\kappa_\beta$ in the two phases are shorter than the cell length L. Here,

$$\kappa_K^2 = 4\pi e^2 (Z_1^2 n_{1K} + Z_2^2 n_{2K}) / \varepsilon_K k_BT$$
$$= 16A(Z_1^2 c_{1K} + Z_2^2 c_{2K}) / \hat{\varepsilon}_K a^2, \quad (4.2)$$

where A is defined by Eq. (3.3) and $\hat{\varepsilon}_K = \varepsilon_K / \varepsilon_c$. Hereafter, the subscript K stands for α or β. The ion densities in the two bulk phases are written as

$$n_{1K} = v_0^{-1} c_{1K}, \quad n_{2K} = v_0^{-1} c_{2K}. \quad (4.3)$$

Far from the interface, the charge density $\rho(z)$ tends to zero and the electric potential $\Phi(z)$ tends to constants, Φ_α and Φ_β. The charge neutrality conditions far from the interface in the two bulk phases are written as

$$Z_1 n_{1K} = Z_2 n_{2K}. \quad (4.4)$$

Since μ_{im}^i vanish far from the interface, the ion densities in the two bulk phases are written as

$$n_{1K} = n_1^0 \exp[-(Z_1 e\Phi_K + \mu_{\text{sol}}^{1K})/k_BT], \quad (4.5)$$

$$n_{2K} = n_2^0 \exp[(Z_2 e\Phi_K - \mu_{\text{sol}}^{2K})/k_BT]. \quad (4.6)$$

We define the solvation chemical potentials in the bulk,

$$\mu_{\text{sol}}^{1K} = \mu_{\text{sol}}^1(\phi_K), \quad \mu_{\text{sol}}^{2K} = \mu_{\text{sol}}^2(\phi_K). \quad (4.7)$$

The charge neutrality condition (4.4) yields

$$\Phi_\alpha - \Phi_\beta = \frac{1}{(Z_1 + Z_2)e} [\Delta\mu_{\alpha\beta}^2 - \Delta\mu_{\alpha\beta}^1]$$
$$= \frac{k_BT}{(Z_1 + Z_2)e} (g_1 - g_2)\Delta\phi. \quad (4.8)$$

Use has been made of the definition (1.2). The composition difference is written as

$$\Delta\phi = \phi_\alpha - \phi_\beta > 0. \qquad (4.9)$$

The first line in Eq. (4.8) is the general expression for the potential difference [15–19], while the second line is a simplified expression under the assumption (2.19). This potential difference depends on the ion density only through ϕ_α and ϕ_β [see Eq. (4.38) below]. Notice that the potential difference arises in the asymmetric case ($g_1 \neq g_2$) only and vanishes in the symmetric case ($g_1 = g_2$). More strongly in our model, we find $\Phi(z) = \rho(z) = 0$ even around the interface for $g_1 = g_2$.

Furthermore, the charge densities in the phase β are reduced as

$$\frac{n_{1\beta}}{n_{1\alpha}} = \frac{n_{2\beta}}{n_{2\alpha}} = \exp\left(-\frac{\epsilon_r}{k_B T}\right). \qquad (4.10)$$

The degree of the ion-density reduction is represented by the energy ϵ_r written as

$$
\begin{aligned}
\epsilon_r &= \frac{Z_2}{Z_1 + Z_2}\Delta\mu_{\alpha\beta}^1 + \frac{Z_1}{Z_1 + Z_2}\Delta\mu_{\alpha\beta}^2 \\
&= \frac{k_B T}{Z_1 + Z_2}(Z_2 g_1 + Z_1 g_2)\Delta\phi. \qquad (4.11)
\end{aligned}
$$

The second line holds under Eq. (2.19) as in the second line of Eq. (4.8). For example, if $\Delta\mu_{\alpha\beta}^1/k_B T = \Delta\mu_{\alpha\beta}^2/k_B T = 10$ and 60, the ion reduction factor becomes $e^{-10} = 2.4 \times 10^{-4}$ and $e^{-60} = 0.67 \times 10^{-26}$, respectively, in the monovalent case. In the latter case, the ion density is virtually zero in the phase β. The Debye-Hückel wave numbers in Eq. (4.2) satisfy

$$\kappa_\beta / \kappa_\alpha = (\varepsilon_\alpha / \varepsilon_\beta)^{1/2} \exp(-\epsilon_r / 2 k_B T). \qquad (4.12)$$

If $\epsilon_r / k_B T$ is considerably larger than unity, we have $n_{1\beta} \ll n_{1\alpha}$, $n_{2\beta} \ll n_{2\alpha}$, and $1/\kappa_\beta \gg 1/\kappa_\alpha$. On the other hand, as we approach the critical point, $\Delta\phi$ and $\epsilon_r / k_B T$ eventually become small, where the heterogeneity in the ion distributions is weak. If g_1 and g_2 are large, this crossover occurs very close to the critical point.

We show numerical results in the monovalent case. In Figs. 3–5, we set $\chi = 2.3$, $g_1 = 4$, $g_2 = 2$, $A = 4$, and $\langle\psi\rangle = 0$ with $L = 100a$. At the boundaries at $z = 0$ and L, we impose the conditions,

$$\psi' = 0, \quad \Phi' = 0. \qquad (4.13)$$

If $\kappa_\beta L \gg 1$, we may realize the interface profiles not affected by the boundary effects. Figure 3 displays the ion densities and the charge density for $c_{1\alpha} = 1.75 \times 10^{-3}$. The charge density changes rather abruptly between the maximum and the minimum on the scale of ξ [42], but slowly tends to zero outside the interval of them on the scale of $1/\kappa_\alpha$ or $1/\kappa_\beta$. We can also see a rounded peak in $c_1(z)$ in the phase α. The latter is due to the factor $\exp(-U)$ where $U = e\Phi/k_B T$ decreases by 0.2 on the left of the interface. This peak tends to disappear for larger g_i. For three values of $c_{1\alpha}$, Figs. 4 and 5 illustrate the electric potential $\Phi(z)$ and the composition deviation $\psi(z)$, respectively. They are consistent with Eq. (4.8). For example, for the case (b) with $c_{1\alpha} = 0.018$ in Figs. 4 and 5, we numerically obtain $\psi_\alpha = 0.3374$, $\psi_\beta = -0.3137$, and ΔU
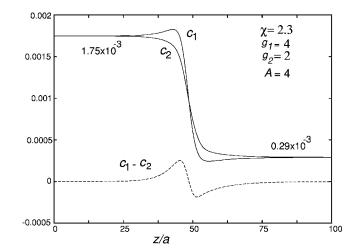

FIG. 3. Normalized ion densities $c_1(z)$ and $c_2(z)$ around an interface where $c_{1\alpha} = c_{2\alpha} = 1.75 \times 10^{-3}$ and $c_{1\beta} = c_{2\beta} = 0.29 \times 10^{-3}$.

$= e(\Phi_\alpha - \Phi_\beta)/k_B T = 0.6410$ to confirm the coincidence of the left-hand and right-hand sides of Eq. (4.8). Furthermore, the ion reduction factor in Eq. (4.10) is $\exp[-3\Delta\phi] = 0.146$ for this case, which is consistent with the numerical value $c_{1\beta} = 0.002\,64$.

Near a water-air interface without ions in air, the microscopic calculations [6] showed a difference between the cation and anion distributions, which decreases in the order of the series: NaI < NaBr < NaCl < NaF in agreement with the order of the depletion-layer-thickness λ_s in Eq. (1.3). The distributions are most different for NaI and almost coincide for NAF. This suggests that the hydration chemical potentials are most different for Na$^+$ and I$^-$ and are nearly equal for Na$^+$ and F$^-$. See the sentences around Eq. (4.20).

B. Charge density and electric potential

Emergence of a charge density around an interface gives rise to a change of the electric potential across the interface. To show this in the case $\kappa_\beta L \gg 1$, we integrate Eq. (2.4) to obtain the electric induction,
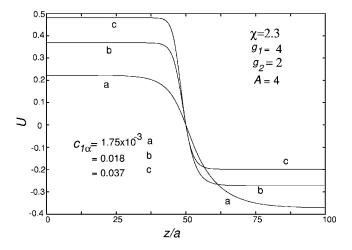

FIG. 4. Normalized electric potential $U(z) = e\Phi(z)/k_B T$ for three cases of $c_{1\alpha} = 1.75 \times 10^{-3}$, 0.018, and 0.037, where we set $\Phi(50a) = 0$.
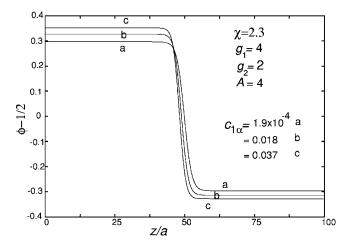
FIG. 5. Order parameter profile $\psi(z) = \phi(z) - 1/2$ for three cases of $c_{1\alpha} = 1.9 \times 10^{-4}$ (a), 0.018 (b), and 0.037 (c). For the smallest $c_{1\alpha}$, $\psi(z)$ is almost equal to the profile without ions.

$$D(z) = -\varepsilon(z)\Phi'(z) = 4\pi \int_{-\infty}^{z} dz' \rho(z'), \qquad (4.14)$$

where the lower bound is pushed to $-\infty$. The z dependence of ε stems from that of ϕ. To ensure $D(\infty) = 0$, we need to require the total charge neutrality condition $\int_{-\infty}^{\infty} dz \rho(z) = 0$. Dividing Eq. (4.14) by ε and integrating it, we obtain

$$\Phi(z) = \Phi_\alpha - 4\pi \int_{-\infty}^{z} dz' \rho(z')[\zeta(z) - \zeta(z')], \quad (4.15)$$

where we introduce

$$\zeta(z) = \int_{z_{\text{int}}}^{z} dz' \frac{1}{\varepsilon(z')}. \qquad (4.16)$$

The right-hand side of Eq. (4.15) is independent of the lower bound z_{int} in Eq. (4.16). However, it is convenient to choose z_{int} as the interface position in the Gibbs construction [43] [see Eq. (4.42) below]; then, $\zeta \cong (z - z_{\text{int}})/\varepsilon_K$ far from the interface where $K = \alpha$ or β in the α or β region. Here $z \int_{-\infty}^{z} dz' \rho(z') \propto z\Phi'(z)$ should tend to zero for large z [since $\rho(z) \propto e^{-\kappa_\beta z}$ as $z \to \infty$], we have

$$\Phi_\alpha - \Phi_\beta = -4\pi \int_{-\infty}^{\infty} dz' \rho(z')\zeta(z'), \qquad (4.17)$$

where the upper bound is also pushed to infinity. We are interested in the potential value at the interface position,

$$\Phi_\alpha - \Phi(z_{\text{int}}) = -4\pi \int_{-\infty}^{z_{\text{int}}} dz' \rho(z')\zeta(z'). \qquad (4.18)$$

As can be inferred from the profile of $c_1 - c_2 = a^3\rho/e$ in Fig. 3, Φ should decrease from the maximum to the minimum point of ρ by a small amount $(\Delta\Phi)_{\text{sol}} \propto n_{1\alpha}$ [42]. For $g_1 > g_2 \gg 1$ with $\Delta\phi \sim 1$, it is estimated as

$$(\Delta\Phi)_{\text{sol}} \sim e n_{1\alpha} \xi^2 \ln(g_1/g_2)/\varepsilon_\alpha. \qquad (4.19)$$

If $\xi \sim a$, we obtain $e(\Delta\Phi)_{\text{sol}}/k_B T \sim c_{1\alpha} A \ln(g_1/g_2)$.

In view of the inequality $|\rho(z)| < 2eZ_1 n_{1\alpha}$, it is surprising that $\Phi_\alpha - \Phi_\beta$ in Eq. (4.8) remains nonvanishing even in the dilute limit of ions. In the low density limit of the ions, therefore, ρ should change over the screening length outside the interval between the extremum points of ρ. Furthermore, if $\kappa_\beta \ll \kappa_\alpha$, the typical variation of Φ in the α region should be smaller than that in the β region by the factor $\varepsilon_\beta\kappa_\beta/\varepsilon_\alpha\kappa_\alpha$ owing to the continuity of $D(z)$ in Eq. (4.14). In the case $\kappa_\beta \ll \kappa_\alpha \ll \xi^{-1}$, the potential decrease Eq. (4.18) behaves as

$$\Phi_\alpha - \Phi(z_{\text{int}}) \cong (\Delta\Phi)_{\text{sol}} + 2\frac{\varepsilon_\beta\kappa_\beta}{\varepsilon_\alpha\kappa_\alpha}\frac{k_B T}{e}\sinh\left(\frac{\Delta U}{2}\right), \qquad (4.20)$$

where $\Delta U = e(\Phi_\alpha - \Phi_\beta)/k_B T$. See discussions below Eq. (4.56). The electric field on the left-hand side of the maximum point of ρ in the α region is negligible in the limit $n_\beta \to 0$. In accord with this result, $\rho = \Phi = 0$ was assumed in the water region in the previous papers [24–27].

C. Grand potential density

We consider the grand potential density in one-dimensional equilibrium situations,

$$\omega(z) = f + \frac{C}{2}|\phi'|^2 - h\phi + \frac{\varepsilon}{8\pi}E^2 + m\mu_{\text{im}}$$
$$+ \sum_{i=1,2} n_i[k_B T(\ln(v_0 n_i) - 1) + \mu_{\text{sol}}^i(\phi) - \mu_i], \qquad (4.21)$$

where μ_{im} is defined by Eq. (2.29) and h, μ_1, and μ_2 are constants (Lagrange multipliers). The grand potential is given by

$$\Omega = \int d\mathbf{r}\,\omega = F - \int d\mathbf{r}\left[h\phi + \sum_{i=1,2} \mu_i n_i\right], \qquad (4.22)$$

where F is the Helmholtz free energy (2.1). If we minimize Ω as a functional of ϕ, n_1, and n_2, we are led to Eqs. (2.26) and (2.27) with Eq. (2.28). To obtain an interface, we impose the boundary condition $\phi \to \phi_K$ ($K = \alpha, \beta$) with $\phi_\alpha > \phi_\beta$ far from the interface.

For the interface solution, we can prove the relation,

$$\frac{d}{dz}[\omega - C|\phi'|^2 - m\mu_{\text{im}}] = -n_1'\mu_{\text{im}}^1 - n_2'\mu_{\text{im}}^2 - \phi' h_{\text{im}}, \qquad (4.23)$$

where the prime denotes taking the derivative d/dz. We may see that the z integration of the right-hand side of Eq. (4.23) vanishes. In fact, if we shift z in $\phi(z)$, $n_i(z)$, and $\Phi(z)$ to $z + \delta\zeta$, the incremental change of F_{im} is

$$\delta F_{\text{im}} = \int d\mathbf{r}[n_1'\mu_{\text{im}}^1 + n_2'\mu_{\text{im}}^2 + \phi' h_{\text{im}}]\delta\zeta. \qquad (4.24)$$

For constant $\delta\zeta$, we have $\delta F_{\text{im}} = 0$ from the translational invariance of the interface position. This is justified if the interface is located very far from the boundary walls. Then

integration of Eq. (4.23) indicates coincidence of the bulk values of $\omega(z)$

$$\omega_\infty = f(\phi_\alpha) - h\phi_\alpha - k_B T n_\alpha$$
$$= f(\phi_\beta) - h\phi_\beta - k_B T n_\beta. \quad (4.25)$$

Here, n_α and n_β are the bulk values of $n = n_1 + n_2$. We have eliminated μ_1 and μ_2 with the aid of $\Sigma_i n_i [\mu_i - k_B T \ln n_i - \mu_{\text{sol}}^i] \to 0$ far from the interface which follows from Eqs. (2.26) and (4.4). The homogeneity of h in Eq. (2.27) yields

$$h = f'(\phi_\alpha) - k_B T(g_1 n_{1\alpha} + g_2 n_{2\alpha})$$
$$= f'(\phi_\beta) - k_B T(g_1 n_{1\beta} + g_2 n_{2\beta}). \quad (4.26)$$

Now Eqs. (4.25) and (4.26) supplemented with Eqs. (2.14) and (4.10) constitute a closed set of equations that determine the equilibrium compositions ϕ_α and ϕ_β, as will be examined in Sec. IV G.

D. Surface tension

In terms of the grand potential density in Eq. (4.21), the surface tension is written as

$$\gamma = \int dz[\omega(z) - \omega_\infty], \quad (4.27)$$

where the integrand tends to zero away from the interface owing to Eq. (4.25). We eliminate μ_1 and μ_2 in $\omega(z)$ using Eq. (2.29) to have a simpler expression,

$$\omega(z) = f + \frac{C}{2}|\phi'|^2 - h\phi - k_B T n + \frac{\varepsilon}{8\pi}E^2 - \rho\Phi. \quad (4.28)$$

Use of Eq. (2.4) gives

$$\gamma = \int dz\left[f(\phi) + \frac{C}{2}|\phi'|^2 - h\phi - k_B T n - \frac{\rho}{2}\Phi - \omega_\infty\right]. \quad (4.29)$$

On the other hand, the surface tension without ions is expressed as

$$\gamma_0 = \int dz\left[f(\phi_0) + \frac{1}{2}C|\phi_0'|^2 - f_0\right], \quad (4.30)$$

where $\phi_0(z)$ is the interface solution without ions, tending to $\phi_{0\alpha}$ and $\phi_{0\beta}$ as $z \to \mp\infty$, respectively. It satisfies [37]

$$f'(\phi_0) - C\phi_0'' = 0$$

$$f(\phi_0) - \frac{1}{2}C|\phi_0'|^2 = f_0 = \text{const.} \quad (4.31)$$

at any z so that $f_0 = f(\phi_{0\alpha}) = f(\phi_{0\beta})$. For the special form of f in Eq. (2.14), we have $h = 0$ (in the zeroth order) and $\phi_{0\alpha} + \phi_{0\beta} = 1$ [48].

Let us consider the excess surface tension,

$$\Delta\gamma = \gamma - \gamma_0. \quad (4.32)$$

In Fig. 6, we show the normalized excess surface tension $a^2 \Delta\gamma/k_B T$ versus $c_{1\alpha}$ at $A = 4$ for $\chi = 3$, 2.3, and 2.05, for
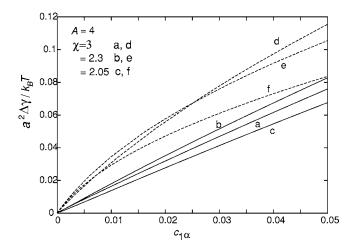

FIG. 6. Normalized excess surface tension $a^2 \Delta\gamma/k_B T$ vs $c_{1\alpha}$ for $\chi = 3$ (a), 2.3 (b), and 2.05 (c) with $g_1 = 4$ and $g_2 = 2$ (solid lines), and for $\chi = 3$ (d), 2.3 (e), and 2.05 (f) with $g_1 = 10$ and $g_2 = 5$ (broken lines).

which $a^2 \gamma_0/k_B T = 0.498$, 0.103, and 0.0773, respectively. Here γ_0 are very different for these values of χ. We set $g_1 = 4$ and $g_2 = 2$ for the curves (a), (b), and (c) (solid lines), while $g_1 = 10$ and $g_2 = 5$ for the curves (d), (e), and (f) (broken lines). We generally find that $\Delta\gamma$ increases with increasing g_i. The linear dependence $\Delta\gamma \propto c_{1\alpha}$ roughly holds at relatively large $c_{1\alpha}$, but the curves depend on the various parameters in a rather complicated manner at smaller $c_{1\alpha}$. The characteristic length λ_s defined by Eq. (1.3) is obtained from $\lambda_s/a = (a^2 \Delta\gamma/k_B T)/c_{1\alpha}$. Then we can see that $\lambda_s/a \sim 2$ for the curves in Fig. 6.

E. Approximations in dilute electrolytes

When n_1 and n_2 are very small, we set

$$\phi(z) = \phi_0(z) + \delta\phi(z), \quad (4.33)$$

where the deviation $\delta\phi(z)$ is assumed to be small. From Eq. (4.31) and the relation $f'(\phi_{0K}) = 0$ the deviations

$$f(\phi_K) - f_0 = \frac{1}{2}k_B T r_K(\phi_K - \phi_{0K})^2 + \cdots \quad (4.34)$$

at $z = \pm\infty$ are of second order in $\delta\phi$, where

$$r_K = f''(\phi_{0K})/k_B T. \quad (4.35)$$

For our f in Eq. (2.14), we have $r_\alpha = r_\beta$, as can be seen from Eq. (A2). Now Eq. (4.25) gives

$$h \cong -k_B T \Delta n/\Delta\phi, \quad (4.36)$$

where Δn is the ion-density difference,

$$\Delta n = n_\alpha - n_\beta = n_\alpha[1 - \exp(-\epsilon_r/k_B T)]. \quad (4.37)$$

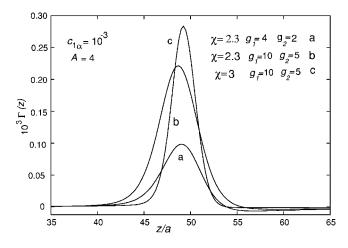From Eq. (4.26), the composition deviations far from the interface are written as

FIG. 7. Normalized integrand $\Gamma(z)$ of Eq. (4.41) for $\chi=2.3$, $g_1=4$, and $g_2=2$ (a), for $\chi=2.3$, $g_1=10$, and $g_2=5$ (b), and for $\chi=3$, $g_1=10$, and $g_2=5$ (c). Its integral with respect to z/a is equal to $a^2\Delta\gamma/k_BT$ in the approximate formula (4.40).

$$\phi_K - \phi_{0K} \cong \frac{1}{r_K}\left[g_1 n_{1K} + g_2 n_{2K} - \frac{\Delta n}{\Delta\phi}\right], \qquad (4.38)$$

where $K=\alpha$, β. This relation is consistent with the results in Fig. 5.

We next devise an approximate formula for $\Delta\gamma$ in the dilute case starting with Eq. (4.29). From Eq. (4.31), we have

$$f(\phi) + \frac{C}{2}|\phi'|^2 = f(\phi_0) + \frac{C}{2}|\phi'_0|^2 + C\frac{d}{dz}(\phi'_0\delta\phi) + \cdots,$$
$$(4.39)$$

where the contributions of second order in $\delta\phi$ are not written. Since the third term on the right-hand side of Eq. (4.39) vanishes on integration, we obtain

$$\frac{\Delta\gamma}{k_BT} \cong \int dz\left[n_\alpha - n(z) - \frac{\Delta n}{\Delta\phi}(\phi_\alpha - \phi(z))\right] \qquad (4.40)$$

to linear order in $\delta\psi$. The integrand tends to zero for large $|z|$.

We introduce the normalized integrand of Eq. (4.40)

$$\Gamma(z) = v_0(n_\alpha - n(z)) - v_0(\Delta n/\Delta\phi)(\phi_\alpha - \phi(z)). \quad (4.41)$$

In Fig. 7, we show $\Gamma(z)$ for three cases with $A=4$ and $c_{1\alpha}=10^{-3}$. It is positive mostly, but has a small negative tail in the phase β (in the region $z/a \gtrsim 55$ here). Numerical values of λ_s/a are 1.84 from Eq. (4.29) and 1.96 from Eq. (4.40) for the curve (a) with $\chi=2.3$, $g_1=4$, and $g_2=2$. They are 4.86 and 4.62 for (b) with $\chi=2.3$, $g_1=10$, and $g_2=5$, and are 3.86 and 3.68 for (c) with $\chi=3$, $g_1=10$, and $g_2=5$, respectively. The differences between these two values are of order 5% at $c_{1\alpha}=10^{-3}$; thus, the approximate formula (4.40) is not very precise at this ion density. Increases in λ_s or $\Delta\gamma$ with increasing g_1 and g_2 are again observed. However, for $g_1=10$ and $g_2=5$, λ_s is larger for (b) with $\chi=2.3$ than for (c) with $\chi=3$, since $\Gamma(z)$ is more broadened for (b) than for (c) in Fig. 7. The same tendency can also be found between the two curves (a) and (b) and between the two curves (d) and (e) at small $c_{1\alpha}$ in Fig. 6. Additional comments are as follows. (i)
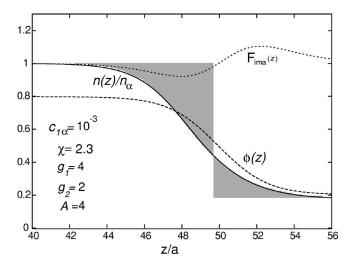

FIG. 8. Normalized ion density $n(z)/n_\alpha$, composition $\phi(z)$, and image factor $F_{\text{ima}}(z)$ for $\chi=2.3$, $g_1=4$, $g_2=2$, and $c_{1\alpha}=10^{-3}$. The gray regions correspond to the two terms in Eq. (4.45).

The contributions from the integral $-\int\rho\Phi/2 = -\int dz\varepsilon E^2/8\pi$ in Eq. (4.29) are at most a few percent of the total contribution in all the calculations. (ii) In the right-hand sides of Eqs. (4.29) and (4.40), we have used the same ϕ and n_{1K} for finite ion densities.

F. Repulsion of ions from an interface

It is convenient to define the interface position z_{int} by

$$\phi_\alpha z_{\text{int}} + \phi_\beta(L - z_{\text{int}}) = \int_0^L dz\,\phi(z), \qquad (4.42)$$

which is the Gibbs construction of the interface position [43]. We use the boundary condition (4.13), which allows the neglecting of the wetting layer. When the distances z_{int} and $L-z_{\text{int}}$ are much longer than the interface thickness and the screening length, Eq. (4.40) may be expressed as

$$\frac{\Delta\gamma}{k_BT} \cong \int_{-\infty}^{z_{\text{int}}} dz[n_\alpha - n(z)] + \int_{z_{\text{int}}}^\infty dz[n_\beta - n(z)], \quad (4.43)$$

where the lower and upper bounds are pushed to infinity. Here, the first term is positive and the second term is negative, with the sum being positive, in our calculations. The second term becomes negligible for small $n(z)$ in the β region $z > z_{\text{int}}$. This occurs in strong ion segregation with considerably large g_1 and g_2. The characteristic length λ_s in Eq. (1.3) is then the thickness of the effective ion-depletion layer in the α region $z < z_{\text{int}}$. In the previous literature, only the first term in Eq. (4.43) has been considered in the thin interface limit $\xi\to 0$.

We illustrate how the two terms in Eq. (4.43) can be interpreted graphically. In Figs. 8–10, we display the normalized ion density $n(z)/n_\alpha$, the composition $\phi(z)$, and the image factor defined by

$$F_{\text{ima}}(z) = \exp[-\mu_{\text{im}}(z)/k_BT], \qquad (4.44)$$

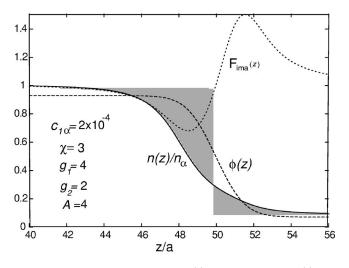which appears in n_1 and n_2 in Eq. (2.30) or Eq. (C2) in the monovalent case. In these figures, the areas of the left and

FIG. 9. Normalized ion density $n(z)/n_\alpha$, composition $\phi(z)$, and image factor $F_{ima}(z)$ for $\chi=3$, $g_1=4$, $g_2=2$, and $c_{1\alpha}=2\times10^{-4}$.

right gray regions divided by a^2 are equal to the first term and the negative of the second term in Eq. (4.43), respectively. The ion density $n(z)$ is shifted to the left of the interface at $z=z_{int}\cong50a$. This means that the ions are repelled from the interface in the phase α.

We furthermore mention detailed characteristic features. (i) In Fig. 8, we set $\chi=2.3$, $c_{1\alpha}=10^{-3}$, $g_1=4$, $g_2=2$, and $A=4$, where the ion density is relatively large and the ion reduction factor ($\sim e^{-1.8}$) is not very small. The first term in Eq. (4.43) is then 158% of the total $\Delta\gamma/k_BT=2.03a^{-2}c_{1\alpha}$, while the second term is −58%. In this case, $F_{ima}(z)\cong1$ at any z so that the image interaction is not important. (ii) In Fig. 9, we set $\chi=3$, $c_{1\alpha}=2\times10^{-4}$, $g_1=4$, $g_2=2$, and $A=4$, where χ is increased and $c_{1\alpha}$ is decreased. The first term of Eq. (4.43) is 138% of the total $\Delta\gamma/k_BT=2.55a^{-2}c_{1\alpha}$ and the image interaction causes considerable reduction of $n(z)$. (iii) In Fig. 10, we set $\chi=3$, $c_{1\alpha}=2.1\times10^{-5}$, $g_1=10$, $g_2=5$, and $A=10$, where g_i and A are increased, the ion density is very
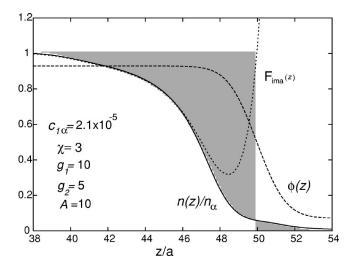

FIG. 10. Normalized ion density $n(z)/n_\alpha$, composition $\phi(z)$, and image factor $F_{ima}(z)$ for $\chi=3$, $g_1=10$, $g_2=5$, and $c_{1\alpha}=2.1\times10^{-5}$. For these parameters, the role of the image factor on $n(z)$ is more dominant than that of the solvation interaction.

small, and $1/\kappa_\alpha=13.3$ is rather long. The first term of Eq. (4.43) is 103.5% of the total $a^2\Delta\gamma/k_BT=7.32c_{1\alpha}$ and the role of the image factor is much intensified.

We discuss the relation between our theory and the Onsager-Samaras theory [25]. For $z_{int}-z\gtrsim\xi$, the image factor behaves as

$$F_{ima}(z)\cong\exp[-D_Ie^{-2\kappa_\alpha|z-z_{int}|}/(z_{int}-z)], \quad (4.45)$$

where $D_I=aA\varepsilon_1\Delta\phi/\pi\varepsilon_c$ in our approximation. The image interaction can be important in the α region for $D_I\gtrsim\xi$ or

$$A\varepsilon_1\Delta\phi/\varepsilon_c\gtrsim\xi/a, \quad (4.46)$$

under which $F_{ima}(z)$ is considerably smaller than unity at $z_{int}-z\sim\xi$. If $\varepsilon_1/\varepsilon_c$, $\Delta\phi$, and ξ/a are of order unity away from the critical point, this condition becomes $A\sim\ell_{Bc}/a\gtrsim1$. Moreover, if $D_I\kappa_\alpha\ll1$ in the dilute limit, the integral of $n_\alpha-n(z)$ in the region $D_I<z_{int}-z<1/\kappa_\alpha$ becomes $n_\alpha D_I\ln(1/D_I\kappa_\alpha)$ and that in the region $\xi<z_{int}-z<D_I$ is of order $n_\alpha D_I$. Thus,

$$\Delta\gamma/k_BT\cong n_\alpha D_I[\ln(1/D_I\kappa_\alpha)+E_I], \quad (4.47)$$

where E_I is a dimensionless constant of order unity. If D_I is set equal to the classical value $e^2/4\varepsilon_\alpha k_BT$ in the case $\varepsilon_\alpha\gg\varepsilon_\beta$, the above result reduces to that by Onsager and Samaras (see Appendix C).

G. Approaching criticality in two-phase states

We are interested in the coexistence curve in the presence of ions in the $\phi-T(\phi-\chi)$ plane [44–46]. We assume the stability of the system against formation of a mesoscopic phase or $\gamma_p<1$ (see Appendix A) [32,39]. We seek the solution of Eqs. (4.25) and (4.26) supplemented with Eq. (4.10) to calculate $\psi_\alpha=\phi_\alpha-1/2$ and $\psi_\beta=\phi_\beta-1/2$. As a parameter representing the amount of the doped ions, there can be many choices. It is convenient to introduce an ion density [50],

$$\bar{n}=(n_\alpha n_\beta)^{1/2}. \quad (4.48)$$

In the monovalent case, we have $v_0\bar{n}=2(c_{1\alpha}c_{1\beta})^{1/2}$ in the dimensionless form so that $n_{1\alpha}=\exp(\epsilon_r/2k_BT)\bar{n}/2$ and $n_{1\beta}=\exp(-\epsilon_r/2k_BT)\bar{n}/2$. We treat $\bar{n}$ and $2-\chi$ as small control parameters characterizing two-phase states with a macroscopic planar interface. If the system is close to the critical point, we may use the Landau expansion $f/k_BT=\tau\psi^2/2+u\psi^4/4+\text{const.}$, where our free energy density Eq. (2.14) gives

$$\tau=(4-2\chi)/v_0, \quad u=16/3v_0. \quad (4.49)$$

We also expand the ion reduction factor in Eq. (4.10) in powers of $\epsilon_r/k_BT\propto\Delta\phi=\psi_\alpha-\psi_\beta$. Some calculations show that the critical condition $\Delta\phi\to0$ is attained at $\tau=\tau_c^{ion}$ with

$$\tau_c^{ion}=[(g_1Z_2+g_2Z_1)/(Z_1+Z_2)]^2\bar{n}. \quad (4.50)$$

Here, $\chi_c^{ion}=2-\tau_c^{ion}v_0/2$ and $\bar{n}=\langle n\rangle(=\text{space average})$ at the critical point, so the above relation is consistent with Eq. (A5). If τ is slightly smaller than τ_c^{ion}, $\tau-\tau_c^{ion}$ represents the reduced temperature at fixed $\bar{n}$ and that ψ_α and ψ_β behave as
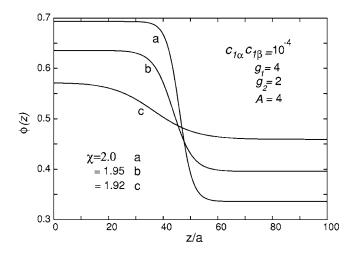
FIG. 11. Composition profiles with varying χ for $g_1=4$, $g_2=2$, $A=4$, and $v_0\bar{n}=0.02$, for which $\chi_c^{\rm ion}=1.91$.

$$\psi_\alpha + \psi_\beta \cong [(g_1 Z_2 + g_2 Z_1)/(Z_1 + Z_2)]^3 \frac{\bar{n}}{3u}, \qquad (4.51)$$

$$\Delta\phi = \psi_\alpha - \psi_\beta \cong 2[(\tau_c^{\rm ion} - \tau)/u]^{1/2}. \qquad (4.52)$$

The first line is the shift of the critical composition multiplied by 2. The second line is the usual mean-field expression.

We next approach the critical point numerically with decreasing χ in two-phase states. As an example, let us set $g_1=4$, $g_2=2$, $A=4$, and $v_0\bar{n}=0.02$. Then the parameter γ_p in Eq. (A6) becomes 0.29 and the critical value of χ becomes $\chi_c^{\rm ion}=2-4.5\langle c_1+c_2\rangle=1.91$ from Eq. (4.50). In Fig. 11, we show the profiles of $\psi(z)$ for $\chi=2$, 1.95, and 1.92 or for $\chi_c^{\rm ion}-\chi=0.09$, 0.04, and 0.01 as the curves (a), (b), and (c). Evidently, the interface thickness increases as $\chi\to\chi_c^{\rm ion}$. For these cases, Eqs. (4.51) and (4.52) yield $\psi_\alpha+\psi_\beta=0.0375$ and $\Delta\phi=1.22(\chi^{\rm ion}-\chi)^{1/2}$ with the aid of Eq. (4.49). For (a), (b), and (c), numerical values are $\psi_\alpha+\psi_\beta=0.0291$, 0.0314, and 0.0303 and $\Delta\phi/(\chi^{\rm ion}-\chi)^{1/2}=1.19$, 1.20, and 1.12, respectively. Therefore, Eqs. (4.51) and (4.52) nicely hold, although n_α and n_β are considerably different for (a) and (b). On the other hand, the normalized potential difference $\Delta U=e(\Phi_\alpha-\Phi_\beta)/k_BT$ is 0.357, 0.240, and 0.112, respectively, in agreement with Eq. (4.8). For $\chi<1.91$ there can only be a solution representing a uniform one-phase state. In Fig. 12, we show $c_1(z)$ and $c_1(z)-c_2(z)$. When the interface thickness ξ much exceeds the screening length, the ion distributions have transition regions with a thickness of order ξ, as it should be the case. The electric double layer at the interface diminishes on approaching the criticality. In addition, the surface tension exhibits the usual mean-field behavior $\gamma\propto(\chi-\chi^{\rm ion})^{3/2}$ near the ion-induced criticality in the mean-field theory.

H. Slow decay of electric potential at small κ_β

When the ion density is very small in the phase β, the potential $\Phi(z)$ slowly changes over the distance of $1/\kappa_\beta$ in the region $z>z_{\rm int}$. Figure 13 displays $U(z)=e\Phi(z)/k_BT$ at
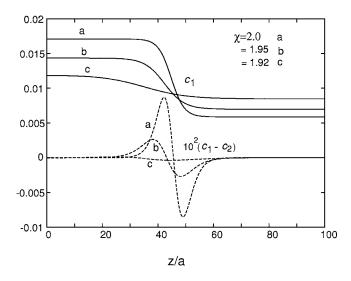

FIG. 12. Normalized ion density $c_1(z)$ and normalized charge density $c_1(z)-c_2(z)$ (multiplied by 100) with varying χ with the same parameter values as in Fig. 11.

$c_{1\alpha}=5\times10^{-4}$ with $\chi=2.3$, $g_1=10$, $g_2=5$, and $A=4$. We use the boundary conditions in Eq. (4.13) with $L=200a$. Since $\phi_\alpha=0.800$ and $\phi_\beta=0.203$, the ion reduction factor in Eq. (4.10) is 0.012, and $c_{1\beta}=5.9\times10^{-6}$, resulting in $1/\kappa_\alpha=5.07a$ and $1/\kappa_\beta=40.0a$.

In the β region not close to the interface ($z-z_{\rm int}\gg\xi$), the composition deviation $\psi(z)-\psi_\beta$ may be neglected and the normalized potential obeys

$$U''(z) = \kappa_\beta^2 F_{\rm ima}(z)\sinh(U(z) - U_\beta), \qquad (4.53)$$

where $U''=d^2U/dz^2$ and $U_\beta=e\Phi_\beta/k_BT$. The image factor defined in Eq. (4.44) behaves as

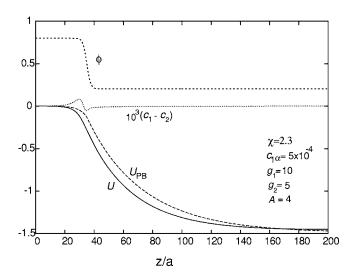FIG. 13. Normalized electric potential $U(z)=e\Phi(z)/k_BT$ (solid line) at small ion density $c_{1\alpha}=5\times10^{-4}$ with $\chi=2.3$, $g_1=10$, $g_2=5$, and $A=4$. Here $c_{1\beta}=5.9\times10^{-6}$ and $\kappa_\beta=2.5\times10^{-2}$. It is compared with the Poisson-Boltzmann solution, Eqs. (4.55) and (4.56), without the image interaction. Also shown are composition profile $\phi(z)$ and the scaled charge density $10^3[c_1(z)-c_2(z)]$.

$$F_{\text{ima}}(z) \cong \exp[D_{\text{I}} e^{-2\kappa_\beta |z-z_{\text{int}}|}/(z-z_{\text{int}})], \qquad (4.54)$$

where $D_{\text{I}} = aA\varepsilon_1\Delta\phi/\pi\varepsilon_c$, as in Eq. (4.45), and $D_{\text{I}} = 0.61a$ in Fig. 13. For example, this factor is equal to 1.038 at $z-z_{\text{int}} = 10a$ in Fig. 13.

If the image factor is set equal to unity, Eq. (4.53) becomes the well-known Poisson-Boltzmann equation which neglects the solvation and image interactions. Its solution, written as $U_{\text{PB}}^>$, is given by

$$U_{\text{PB}}^>(z) = U_\beta + 2\ln\left[\frac{1+d_\beta e^{-\kappa_\beta|z-z_{\text{int}}|}}{1-d_\beta e^{-\kappa_\beta|z-z_{\text{int}}|}}\right], \qquad (4.55)$$

in the region $z > z_{\text{int}}$. If β is changed to α in Eq. (4.55), the Poisson-Boltzmann solution is also obtained in the α region, which is written as $U_{\text{PB}}^<$. We require the continuity of the electric potential and the electric induction, $U_{\text{PB}}^> = U_{\text{PB}}^<$ and $\varepsilon_\beta dU_{\text{PB}}^>/dz = \varepsilon_\alpha dU_{\text{PB}}^</dz$, at $z = z_{\text{int}}$. We then connect the two one-sided solutions,

$$U_{\text{PB}}(z) = U_{\text{PB}}^>(z) \quad (z > z_{\text{int}})$$
$$= U_{\text{PB}}^<(z) \quad (z < z_{\text{int}}), \qquad (4.56)$$

which decreases from U_α at $z = -\infty$ to U_β at $z = \infty$ by $\Delta U = e(\Phi_\alpha - \Phi_\beta)/k_B T$. In Fig. 13, we plot U_{PB} thus obtained with $d_\beta = 0.328$. If $\varepsilon_\beta \kappa_\beta / \varepsilon_\alpha \kappa_\alpha \ll 1$, d_β and $U_\alpha - U_{\text{PB}}(z_{\text{int}})$ are given by $\sinh(\Delta U/4)$ (close to the above value) and the first term on the right-hand side of Eq. (4.20) multiplied by $k_B T/e$, respectively.

Comparing U and U_{PB}, we recognize the following. (i) In the β region, U relaxes to U_β slightly faster than U_{PB} due to the image factor in Eq. (4.54). (ii) The curve of U is shifted into the α region, as compared to U_{PB}, and the decrease of U in the α region $U_\alpha - U(z_{\text{int}})$ is considerably larger than that of U_{PB} in Eq. (4.56). These are due to the charge density created by the asymmetric solvation interaction near the interface, [see Eqs. (4.19) and (4.20)]. (iii) Nevertheless, the small negative tail of the charge density $\rho(z)(\cong -\varepsilon_\beta \Phi''/4\pi)$ in the β region (at least for $z-z_{\text{int}} \gtrsim 1/\kappa_\beta$) is correctly described by the Poisson-Boltzmann theory.

In Fig. 14, we plot the potential reduction ratio $R_p \equiv [\Phi_\alpha - \Phi(z_{\text{int}})]/(\Phi_\alpha - \Phi_\beta) = [U_\alpha - U(z_{\text{int}})]/\Delta U$ in the α region as a function of $c_{1\alpha}$ with $A = 4$ for three cases. It is around 0.4 for weak ion segregation at $\chi = 2.3$, $g_1 = 4$, and $g_2 = 2$ on the curve (a). However, it decreases with decreasing $c_{1\alpha}$ for strong ion segregation with $g_1 = 10$ and $g_2 = 5$ on the curves (b) and (c).

I. Hydrophilic and hydrophobic ions

If hydrophilic and hydrophobic ions are in aqueous solutions, we have $\Delta\mu_{\alpha\beta}^1 > 0$ and $\Delta\mu_{\alpha\beta}^2 < 0$ [14,17] or $g_1 > 0$ and $g_2 < 0$ under Eq. (2.19). With decreasing g_2, the potential difference (4.8) becomes larger and ϵ_r in Eq. (4.10) can even change its sign for this case. In Fig. 15, we set $g_1 = 4$ and $g_2 = -4$ with $c_{1\alpha} = 10^{-3}$, where $\epsilon_r = 0$ and the bulk ion densities far from the interface coincide. We can see that c_1 exhibits a maximum in the α region and a minimum in the β region, while c_2 has extremums in the reverse regions. Thus the relative charge density $(c_1 - c_2)/c_{1\alpha}$ is more intensified than
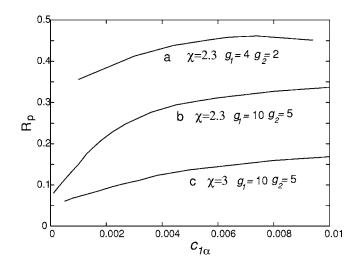

FIG. 14. Potential reduction ratio in the α region $R_p = [\Phi_\alpha - \Phi(z_{\text{int}})]/(\Phi_\alpha - \Phi_\beta)$ versus $c_{1\alpha}$, where $\chi = 2.3$, $g_1 = 4$, and $g_2 = 2$ (a), $\chi = 2.3$, $g_1 = 10$, and $g_2 = 5$ (b), and $\chi = 3$, $g_1 = 10$, and $g_2 = 5$ (c).

in the case of $g_1 > g_2 > 0$. Interestingly, the integral of the deviation $c_1 + c_2 - 2c_{1\alpha}$ is positive due to the image interaction in the β region in this case. That is, the ions are absorbed onto the interface on the average and λ_s in Eq. (1.3) becomes $-3.54a$.

V. SUMMARY AND REMARKS

We have introduced the solvation effects at low ion densities into electrolyte theory in the simplest manner, neglecting ion association [2]. We have then examined the ion distributions, the electric potential, and the composition profile around an interface in polar binary mixtures in the Ginzburg-Landau scheme. We have derived a number of general relations. They are worth experimental investigation particularly near the critical point. Numerical calculations have been per-
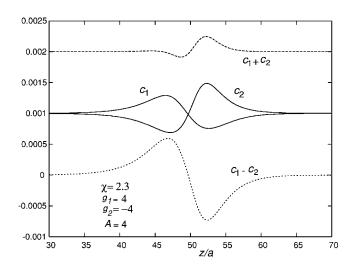

FIG. 15. Normalized ion densities c_1 and c_2 around an interface, where $g_1 = 4$, $g_2 = -4$, $\chi = 2.3$, and $A = 4$. The first species is hydrophilic and the second one is hydrophobic. Also shown are $c_1 - c_2 = a^3\rho/e$ and $c_1 + c_2 = a^3 n$. A marked electric double layer is formed here.

formed in one dimension and in the monovalent case only.

The ingredients of our theory are as follows.

(i) The dielectric constant in Eq. (2.4) is dependent on the composition and is inhomogeneous. Though we have treated a moderate case of $\varepsilon_1/\varepsilon_0 = 4/3$, the ratio $\varepsilon_1/\varepsilon_0$ can be of order 80 in aqueous solutions. Such very strong composition dependence should lead to various effects not well recognized so far. We mention a paper pointing out its relevance in first-order swelling transition of charged gels [51].

(ii) The solvation effects are taken into account in Eq. (2.13) with the composition-dependent solvation chemical potentials in Eq. (2.19). The resultant interaction in the free energy F is bilinear and characterized by dimensionless parameters g_i dependent on the ion species i. A shift of the coexistence curve of the composition follows from this coupling [32]. Intriguing is the asymmetric case $g_1 \neq g_2$, where a potential difference arises at an interface. In one-phase states, this asymmetry can lead to a peak in the structure factor of the composition fluctuations at an intermediate wave number, as summarized in Appendix A. There can even be a mesoscopic phase [39], which can possibly occur in the case of strongly asymmetric salt with large $g_1 - g_2$ (say, salt composed of small cations and relatively large anions with distinctly different solvation powers) [32]. Notice that g_i can be negative for hydrophobic ions. Also we stress that the critical fluctuations give rise to attractive interactions among the ions as shown in Eqs. (A7) and (A8), whose physical consequences should be examined in future.

(iii) The image interaction is shown to arise from general inhomogeneous dielectric constant and is expressed in the integral form in Eq. (2.21) or Eq. (3.7), though our expression can be used only for weak or moderate inhomogeneity. As discussed in Sec. III, it can dominate over the solvation interaction for $A \gg 1$, at very small ion densities, and far below the critical point.

The charge effects become very complex with these new ingredients and our present results are still fragmentary. We mention related problems.

(i) There can be an electric double layer and a potential difference at an interface in general charged systems, including low-molecular-weight fluids (as in this paper), complex fluids, gels, and even liquid metals. In particular, solvation effects in microemulsion systems and charged colloidal systems are of great interest.

(ii) Wetting transitions should be greatly influenced by ions [52,53]. If the wetting layer is more polar than the outer fluid, ions can even be confined in the layer for $\Delta\mu^i_{\alpha\beta} \gg k_B T$ [see Eq. (1.2)].

(iii) We mention dynamical problems. Time evolution of the ion distributions is a slow process due to slow ion diffusion [19]. Phase-separation processes should also be influenced by ions which are more strongly segregated than the solvent composition for large g_i. We already examined the effect of a very small amount of ions on nucleation in a metastable fluid in a less polar phase. There, the nucleation barrier is decreased by $\Delta\mu^i_{\alpha\beta}$ in Eq. (1.2) for shallow quenching [22]. Ion-induced nucleation plays a decisive role in atmospheric phenomena.

(iv) Recently, we examined solvation effects of charged particles in liquid crystals [33,54]. In nematic states, the di-

electric tensor is anisotropically dependent on the director orientation and, as a result, the electric field of ions distorts the orientation over long distances and sometimes create nanometer scale defects.

APPENDIX A: FLUCTUATIONS IN ONE-PHASE STATES

We consider small plane-wave fluctuations in a near-critical one-phase state, where the inhomogeneity in the dielectric constant can be neglected ($\varepsilon = \varepsilon_c$) to leading order. Retaining the Fourier components with wave numbers much larger than the inverse system size $1/L$, we first write the fluctuation contributions to F in the bilinear order as [32]

$$\delta F = \int_{\mathbf{q}} \left[\frac{1}{2}(f'' + Cq^2)|\phi_{\mathbf{q}}|^2 + \frac{2\pi}{\varepsilon_c q^2}|\rho_{\mathbf{q}}|^2 + k_B T \right. $$
$$\left. \times \sum_{i=1,2} \left(\frac{|n_{i\mathbf{q}}|^2}{2n_i} - (g_i - Z_i^2 I_q)n_{i\mathbf{q}}\phi_{\mathbf{q}}^* \right) \right], \quad (A1)$$

where $\int_{\mathbf{q}} \cdots = (2\pi)^{-3}\int d\mathbf{q} \cdots$ denotes the integration over the wave vector $\mathbf{q}$ and

$$f'' = \frac{\partial^2 f}{\partial \phi^2} = \frac{k_B T}{v_0}\left[\frac{1}{\phi(1-\phi)} - 2\chi \right] \quad (A2)$$

in our model. The correlation length is given by $\xi = (C/f'')^{1/2}$ for the case without ions. The $\phi_{\mathbf{q}}$, $n_{i\mathbf{q}}$, and $\rho_{\mathbf{q}}$ are the Fourier transformations of $\phi(\mathbf{r})$, $n_i(\mathbf{r})$, and $\rho(\mathbf{r})$, respectively. The n_i in the last term of Eq. (A1) are the average ion densities satisfying $Z_1 n_1 = Z_2 n_2$ from the charge neutrality. The terms proportional to I_q arise from the image interaction, where Eq. (2.24) yields

$$I_q = (4\pi B_0/k_B T)q \tan^{-1}(q/2\kappa), \quad (A3)$$

so that $I_q \propto q^2$ for $q \ll \kappa$. The terms from the image interaction are negligible at any q in one-phase states, so they will be omitted hereafter.

Elimination of the ion-density fluctuations yields the composition structure factor in the mean-field theory,

$$\frac{k_B T}{S(q)} = f'' - \Delta r_{\text{ion}} + Cq^2\left[1 - \frac{\gamma_p^2 \kappa^2}{\kappa^2 + q^2} \right], \quad (A4)$$

where κ is the Debye-Hückel wave number and Δr_{ion} is the ion-induced shift,

$$\Delta r_{\text{ion}} = k_B T(Z_2 g_1 + Z_1 g_2)^2 n/(Z_1 + Z_2)^2. \quad (A5)$$

The shift becomes significant for large g_i even for small $n = n_1 + n_2$. This is consistent with the experimental fact that

even a small amount of salt greatly shifts the liquid-liquid coexistence curve [44–47]. The dimensionless parameter γ_p represents the asymmetry of the solvation in the two components,

$$\gamma_p = |g_1 - g_2|(k_B T/4\pi C \ell_B)^{1/2}/(Z_1 + Z_2)$$
$$= |g_1 - g_2|/[4(Z_1 + Z_2)\sqrt{\chi A}], \qquad (A6)$$

where we have used Eqs. (2.18) and (3.3) in the second line. For $\gamma_p > 1$, $S(q)$ is maximum at an intermediate wave number and formation of a mesoscopic phase can be predicted below the transition point [32,33,39]. For $\gamma_p < 1$, $S(q)$ is maximum at $q=0$ and the usual critical point still exists.

We may also eliminate the critical fluctuations in F by setting $(f'' + Cq^2)\phi_q = k_B T \Sigma_{i=1,2} g_i n_{i\mathbf{q}}$. The resultant free energy F_{ion} for the ions only is expressed in the real space as

$$F_{\text{ion}} = k_B T \int d\mathbf{r} \sum_i n_i [\ln(v_0 n_i) - 1] + \frac{1}{2} \int d\mathbf{r} \int d\mathbf{r}'$$
$$\times \sum_{i,j} V_{ij}(|\mathbf{r} - \mathbf{r}'|) n_i(\mathbf{r}) n_j(\mathbf{r}'), \qquad (A7)$$

where the first entropic terms are not expanded with respect to the ion-density deviations and $V_{ij}(r)$ are the interaction potentials,

$$V_{ij}(r) = Q_i Q_j \frac{1}{\varepsilon_c r} - \frac{(k_B T)^2}{4\pi C} g_i g_j \frac{e^{-r/\xi}}{r}, \qquad (A8)$$

with $Q_1 = Z_1 e$ and $Q_2 = -Z_2 e$. The second term in Eq. (A8) is the effective interaction mediated by the critical fluctuations. Among the ions of the same species ($i=j$) it is attractive and dominates over the first Coulomb repulsive term in the intermediate range $a \lesssim r \lesssim \xi$ if

$$g_i^2 > 4\pi C Z_i^2 e^2/\varepsilon_c (k_B T)^2 \sim 4\pi Z_i^2 \ell_{Bc}/a. \qquad (A9)$$

Under the above strong solvation condition, there should be a tendency of aggregation even among ions of the same species. This effect might explain a number of observations of microheterogeneities in near-critical binary mixtures containing salt [47].

APPENDIX B: IMAGE POTENTIAL AND GENERALIZATION

(i) First, let two fluid phases α and β with dielectric constants ε_α and ε_β be separated by a planar interface with the phase α in the region $z<0$. Here $\varepsilon_\alpha > \varepsilon_\beta$ and the thin interface limit is taken. We place an ion with charge Q at a position $\mathbf{r}_0 = (x_0, y_0, z_0)$ in the phase α ($z_0 < 0$). The resultant electric potential Ψ should satisfy the surface condition,

$$\varepsilon_\alpha \Psi'(-0) = \varepsilon_\beta \Psi'(+0), \qquad (B1)$$

where $\Psi' = d\Psi/dz$. Then, Ψ in the phase α ($z<0$) is written as [49]

$$\Psi(\mathbf{r}, \mathbf{r}_0) = \frac{Q}{\varepsilon_\alpha |\mathbf{r} - \mathbf{r}_0|} + \frac{\varepsilon_\alpha - \varepsilon_\beta}{\varepsilon_\alpha + \varepsilon_\beta} \frac{Q}{\varepsilon_\alpha |\mathbf{r} - \bar{\mathbf{r}}_0|}, \qquad (B2)$$

where $\bar{\mathbf{r}}_0 = (x_0, y_0, -z_0)$ is the image position in the phase β. The second term is produced by the polarization of the di-

electric medium. As $\mathbf{r} \to \mathbf{r}_0$, it follows the repulsive potential of the ion dependent on $z_0 (<0)$,

$$\Phi_\alpha(z_0) = \frac{\varepsilon_\alpha - \varepsilon_\beta}{2(\varepsilon_\alpha + \varepsilon_\beta)\varepsilon_\alpha} \frac{Q^2}{|z_0|}, \qquad (B3)$$

which tends to $Q^2/4\varepsilon_\alpha |z_0|$ in the case $\varepsilon_\alpha \gg \varepsilon_\beta$. For the electrolyte, Onsager and Samaras [25] argued that the other ions give rise to a decaying factor $\exp(-2\kappa |z_0|)$, where κ is the Debye-Hückel wave number in the bulk phase α and the image potential should be changed to

$$\Phi_\alpha(z_0) = \frac{\varepsilon_\alpha - \varepsilon_\beta}{2(\varepsilon_\alpha + \varepsilon_\beta)\varepsilon_\alpha} \frac{Q^2}{|z_0|} e^{-2\kappa |z_0|}. \qquad (B4)$$

(ii) Second, we place a charge in the less polar phase β ($z_0 > 0$). This situation is relevant when there are appreciable ions in the phase β or for not very small ion reduction factor in Eq. (4.10). Exchange of α and β in Eq. (B4) gives the image potential in the phase β,

$$\Phi_\beta(z_0) = -\frac{\varepsilon_\alpha - \varepsilon_\beta}{2(\varepsilon_\alpha + \varepsilon_\beta)\varepsilon_\beta} \frac{Q^2}{z_0}, \qquad (B5)$$

which is attractive to the interface and tends to $-Q^2/4\varepsilon_\beta z_0$ in the case $\varepsilon_\alpha \gg \varepsilon_\beta$. The coefficient in Eq. (B5) is larger than that in Eq. (B4) by the factor $\varepsilon_\alpha/\varepsilon_\beta$, which can be very large. However, Eq. (B5) should be much reduced in the presence of a solvation shell composed of polar molecules of the species A [12–14]. See the discussion below Eq. (2.20) for the background of this picture. In electrostatics [49], a polar spherical layer enclosing a charge weakens the electric field acting on the charge by the factor $3\varepsilon_\beta/(2\varepsilon_\beta + \varepsilon_A')$, leading to

$$\Phi_\beta(z_0) = -\frac{\varepsilon_\alpha - \varepsilon_\beta}{2(\varepsilon_\alpha + \varepsilon_\beta)\varepsilon_\beta} \frac{3\varepsilon_\beta}{2\varepsilon_\beta + \varepsilon_A'} \frac{Q^2}{z_0}, \qquad (B6)$$

where $\varepsilon_A'(\sim \varepsilon_A)$ is the effective dielectric constant in the layer. The coefficient in Eq. (B6) is of the same order as that in Eq. (B3) in the case $\varepsilon_\alpha \sim \varepsilon_A' \sim \varepsilon_A \gg \varepsilon_\beta$.

(iii) Third, we should recognize that an image potential Φ_I arises generally when the dielectric constant ε varies in space. We demonstrate it near the critical point, where the deviation $\delta\varepsilon = \varepsilon - \varepsilon_c$ from its critical value ε_c is small. Neglecting the boundary effect, we solve $\nabla \cdot \varepsilon \nabla \Psi = -4\pi Q \delta(\mathbf{r} - \mathbf{r}_0)$ in powers of $\delta\varepsilon$. The deviation $\delta\Psi = \Psi - Q/\varepsilon_c |\mathbf{r} - \mathbf{r}_0|$ reads

$$\delta\Psi(\mathbf{r}, \mathbf{r}_0) = \frac{Q}{4\pi\varepsilon_c^2} \int d\mathbf{r}' \frac{\nabla' \delta\varepsilon(\mathbf{r}')}{|\mathbf{r} - \mathbf{r}'|} \cdot \nabla' \frac{1}{|\mathbf{r}' - \mathbf{r}_0|} \qquad (B7)$$

to linear order in $\delta\varepsilon$. Taking the limit $\mathbf{r} \to \mathbf{r}_0$, we find the image potential,

$$\Phi_I(\mathbf{r}_0) = \frac{Q^2}{8\pi\varepsilon_c^2} \int d\mathbf{r}' \nabla' \delta\varepsilon(\mathbf{r}') \cdot \nabla' \frac{1}{|\mathbf{r}' - \mathbf{r}_0|^2}. \qquad (B8)$$

In particular, if a planar interface with thickness ξ is located at $z \cong 0$, $\varepsilon(z)$ depends only on z and the integrations over x' and y' are performed to give

$$\Phi_I(z_0) = \frac{Q^2}{4\varepsilon_c^2} \int dz' \frac{1}{z_0 - z'} \frac{d}{dz'} \delta\varepsilon(z'), \qquad (B9)$$

where we use $\int dx \int dy (x^2+y^2+z^2)^{-2} = \pi/z^2$. For $|z_0| \gg \xi$, the above expression becomes

$$\Phi_I(z_0) = -\frac{\varepsilon_\alpha - \varepsilon_\beta}{4\varepsilon_c^2} \frac{Q^2}{z_0}, \qquad (B10)$$

which is applicable both in phases α and β. In the electrolyte, the two functions in Eq. (B7), $1/|\mathbf{r}'-\mathbf{r}|$ and $1/|\mathbf{r}'-\mathbf{r}_0|$, should be replaced by $e^{-\kappa|\mathbf{r}'-\mathbf{r}|}/|\mathbf{r}'-\mathbf{r}|$ and $e^{-\kappa|\mathbf{r}'-\mathbf{r}_0|}/|\mathbf{r}'-\mathbf{r}_0|$, respectively, resulting in Eq. (3.7). See the discussion on the choice of κ below Eq. (3.7).

In passing, we note that the electric potential in a finite system can be expressed in terms of the Green's function satisfying $\nabla^2 G(\mathbf{r},\mathbf{r}') = -4\pi\delta(\mathbf{r}-\mathbf{r}')$ under the given boundary conditions. At fixed surface charges, its derivative with respect to z vanishes at $z=0$ and L in the geometry of Fig. 1, where $G(\mathbf{r},\mathbf{r}') = G(z,z',\mathbf{s})$ with $\mathbf{s} = (x-x',y-y')$. Its Fourier transformation $G_k(z,z') = \int d\mathbf{s} G(z,z',\mathbf{s})e^{i\mathbf{k}\cdot\mathbf{s}}$ is calculated as

$$G_k(z,z') = \frac{2\pi}{k} e^{-k|z-z'|} + \frac{4\pi}{k(\sigma^2-1)} [\cosh[k(z-z')]$$
$$+ \sigma \cosh[k(z+z'-L)]], \qquad (B11)$$

where $\sigma = e^{kL}$. It is obvious that $1/|\mathbf{r}'-\mathbf{r}_0|^2$ in Eq. (B8) should be replaced by $G(\mathbf{r}',\mathbf{r}_0)^2$.

APPENDIX C: DIMENSIONLESS EQUATIONS

We write down the dimensionless equilibrium equations in one-dimensional cases. Here, the z coordinate is measured in units of a. Using Eq. (2.14), we rewrite Eq. (2.27) as

$$\frac{v_0 h}{k_B T} = \ln\left[\frac{1+2\psi}{1-2\psi}\right] - 2\chi\psi - \chi\psi'' - \frac{\hat{\varepsilon}_1}{32A}U'^2 - (g_1 c_1 + g_2 c_2)$$
$$+ A\hat{\varepsilon}_1 \hat{I} c. \qquad (C1)$$

For $Z_1 = Z_2 = 1$, Eq. (2.30) becomes

$$c_1 = c_1^0 \exp[g_1\psi - U - A\hat{\varepsilon}_1 \hat{I}\psi],$$

$$c_2 = c_2^0 \exp[g_2\psi + U - A\hat{\varepsilon}_1 \hat{I}\psi], \qquad (C2)$$

where $\hat{\varepsilon}_1 = \varepsilon_1/\varepsilon_c$, A is defined by Eq. (3.3), $\psi'' = d^2\psi/dz^2$, and $U' = dU/dz$. The $v_0 h/k_B T$, c_1^0, and c_2^0 are constants in equilibrium. Here, $\hat{I}$ is the linear operator arising from the image interaction

$$(\hat{I}\psi)(z) = \int \frac{dz'}{\pi} \frac{e^{-2\kappa a|z-z'|}}{z-z'} \frac{d\psi(z')}{dz'}. \qquad (C3)$$

From Eq. (2.4), we obtain the equation for U,

$$-\frac{d}{dz}[1 + \hat{\varepsilon}_1\psi]\frac{d}{dz}U = 16A(c_1 - c_2). \qquad (C4)$$

[1] *Electrostatic Effects in Soft Matter and Biophysics*, edited by C. Holm, P. Kekicheff, and R. Podgornik, NATO Science Series II (Kluwer Academic, Dordrecht, 2001), Vol. 46.

[2] Y. Levin and M. E. Fisher, Physica A **225**, 164 (1996); Y. Levin, Rep. Prog. Phys. **65**, 1577 (2002).

[3] J. N. Israelachvili, *Intermolecular and Surface Forces* (Academic Press, London, 1991).

[4] Y. Marcus, *Ion Solvation* (Wiley, New York, 1985).

[5] P. B. Balbuena, K. P. Johnston, and P. J. Rossky, J. Phys. Chem. **100**, 2706 (1996).

[6] P. Jungwirth and D. J. Trobias, J. Phys. Chem. B **105**, 10468 (2001); **106**, 6361 (2002).

[7] M. Born, Z. Phys. **1**, 45 (1920). The right-hand side of Eq. (1.1) is simply the integration of the electrostatic energy $\varepsilon E(r)^2/8\pi$ in the region $R_{ion}^i < r < \infty$, where $E(r) = -Ze/\varepsilon r^2$ is the electric field at distance r from the ion center.

[8] Y. Marcus, Chem. Rev. (Washington, D.C.) **88**, 1475 (1988).

[9] D. P. Fernandez, A. R. H. Goodwin, E. W. Lemmon, J. M. H. Levet Sengers, and R. C. Williams, J. Phys. Chem. Ref. Data **26**, 1125 (1997).

[10] P. Debye and K. Kleboth, J. Chem. Phys. **42**, 3155 (1965).

[11] The free energy needed for electrostriction decreases with increasing the background composition ϕ, of the more polar component. This fact is particularly important in ion-induced nucleation, see Ref. [22].

[12] M. H. Abraham, J. Liszi, and L. Meszaros, J. Chem. Phys. **70**, 2491 (1979).

[13] L. Sandberg and O. Edholm, J. Chem. Phys. **116**, 2936 (2002).

[14] T. Osakai and K. Ebina, J. Phys. Chem. B **102**, 5691 (1998).

[15] M. Gros, S. Gromb, and C. Gavach, J. Electroanal. Chem. Interfacial Electrochem. **89**, 29 (1978).

[16] J. Koryta, Electrochim. Acta **24**, 293 (1979); , **29**, 445 (1984).

[17] Le Quoc Hung, J. Electroanal. Chem. Interfacial Electrochem. **115**, 159 (1980).

[18] T. Kakiuchi, Anal. Chem. **68**, 3658 (1996).

[19] H. Jensen, V. Devaud, J. Josserand, and H. H. Girault, J. Electroanal. Chem. **537**, 77 (2002).

[20] C. T. R. Wilson, Philos. Trans. R. Soc. London, Ser. A **189**, 265 (1897).

[21] J. J. Thomson, *Conduction of Electricity through Gases* (Cambridge University Press, Cambridge, 1906), Sec. 92. Thomson predicted formation of a liquidlike hydration shell layer around an ion in gaseous water.

[22] H. Kitamura and A. Onuki, J. Chem. Phys. **123**, 124513 (2005). One of the main results in this work is that the solvent density in the vicinity of a small ion can be of the order of a liquid density in a gaseous polar one-component fluid. In this situation, the Born formula using the dielectric constant of gas is a poor approximation.

[23] S. Durand-Vidal, J. P. Simonin, and P. Turq, *Electrolytes at Interfaces* (Kluwer, Dordrecht, 2000).

[24] C. Wagner, Phys. Z. **25**, 474 (1924).

[25] L. Onsager and N. N. T. Samaras, J. Chem. Phys. **2**, 528 (1934).

[26] Y. Levin, J. Chem. Phys. **113**, 9722 (2000).

[27] Y. Levin and J. E. Flores-Mena, Europhys. Lett. **56**, 187 (2001).

[28] H. Ohshima and H. Matsubara, Colloid Polym. Sci. **282**, 1044 (2002).

[29] N. Matubayasi, H. Matsuo, K. Yamamoto, S. Yamaguchi, and A. Matuzawa, J. Colloid Interface Sci. **209**, 398 (1999).

[30] Wei Lun Hsin, Yu-Jane Sheng, Shi-Yow Lin, and Heng-Kwong Tsao, Phys. Rev. E **69**, 031605 (2004).

[31] S. A. Safran, *Statistical Thermodynamics of Surfaces, Interfaces, and Membranes* (Westview Press, 2003).

[32] A. Onuki and H. Kitamura, J. Chem. Phys. **121**, 3143 (2004).

[33] A. Onuki, in *Nonlinear Dielectric Phenomena in Complex Liquids*, edited by S. J. Rzoska, NATO Science Series II (Kluwer Academic, Dordrecht, 2004), Vol. 157.

[34] The density of dipole pairs can increase significantly even at low ion densities when the Bjerrum length $e^2/\varepsilon k_B T$ is much longer than the molecular size a, see Ref. [2].

[35] If $\varepsilon_A \gg \varepsilon_B$, we have $\varepsilon_1 \gg \varepsilon_0$ and $\varepsilon_1/\varepsilon_c \cong 1/\phi_c$ with ε_c and ϕ_c being the critical values.

[36] We may choose the potential difference $\Phi_L - \Phi_0$ as a control parameter in the geometry of Fig. 1, see Ref. [33]. Then, the surface charges are fluctuating quantities and the relevant electrostatic free energy should be $F_e = -\int d\mathbf{r} \mathbf{D} \cdot \mathbf{E}/8\pi$. With this choice the chemical-potential contributions in Eqs. (2.11) and (2.12) remain unchanged.

[37] A. Onuki, *Phase Transition Dynamics* (Cambridge University Press, Cambridge, 2002).

[38] I. Borukhov, D. Andelman, and H. Orland, Phys. Rev. Lett. **79**, 435 (1997). The steric effect due to ions yields terms $C_s^i n_i \psi$ in the free energy density at low salt densities with $C_s^i \sim 1$ for $R_{shell}^i \sim a$. Notice that these terms can be included into the solvation terms in Eq. (2.13).

[39] V. M. Nabutovskii, N. A. Nemov, and Yu. G. Peisakhovich, Phys. Lett. **79**, 98 (1980); Zh. Eksp. Teor. Fiz. **79**, 2196 (1980) [Sov. Phys. JETP **52**, 111 (1980)]; Mol. Phys. **54**, 979 (1985).

[40] Here $(g_i)_{Born} = Z_i^2 \ell_{Bc} \varepsilon_1/R_{ion}^i \varepsilon_c$ in terms of ℓ_{Bc} in Eq. (3.4), so $(g_i)_{Born}/Z_i^2$ can even be of order 100.

[41] P. G. de Gennes, Rev. Mod. Phys. **57**, 827 (1985).

[42] If $g_1 > g_2 \gg 1/\Delta\phi$, the distance of the maximum (minimum) point from the interface position (in the Gibbs sense) is of order $\xi \ln(g_1 \Delta\phi)[\xi \ln(g_2 \Delta\phi)]$ from the balance $g_i(\phi_\alpha - \phi) \sim g_i \Delta\phi \exp[2(z-z_{int})/\xi] \sim 1$.

[43] D. Chandler, *Introduction to Modern Statistical Mechanics* (Oxford University Press, Oxford, 1987).

[44] E. L. Eckfeldt and W. W. Lucasse, J. Phys. Chem. **47**, 164 (1943).

[45] B. J. Hales, G. L. Bertrand, and L. G. Hepler, J. Phys. Chem. **70**, 3970 (1966).

[46] V. Balevicius and H. Fuess, Phys. Chem. Chem. Phys. **1**, 1507 (1999).

[47] M. A. Anisimov, J. Jacob, A. Kumar, V. A. Agayan, and J. V. Sengers, Phys. Rev. Lett. **85**, 2336 (2000).

[48] We may set $\mu_0 = f'(\phi_{0K}) = 0$ in the zeroth order without loss of generality if we redefine $f - \mu_0\phi$ as f.

[49] L. D. Landau and E. M. Lifshitz, *Electrodynamics of Continuous Media* (Pergamon, New York, 1984), Vol. 8.

[50] We may choose n_α as the control parameter. Then, if $\bar{n}$ is replaced by n_α, Eqs. (4.51) and (4.52) still hold asymptotically. But they are applicable only much closer to the critical point, where $n_{1\alpha} \cong n_{1\beta}$.

[51] Yu. Kramarenko, I. Ya. Erukhimovich, and A. R. Khokhlov, Macromol. Theory Simul. **11**, 462 (2002).

[52] R. F. Kayser, Phys. Rev. Lett. **56**, 1831 (1986).

[53] N. A. Denesyuk and J. P. Hansen, J. Chem. Phys. **121**, 3613 (2004).

[54] A. Onuki, J. Phys. Soc. Jpn. **73**, 511 (2004).